DOI: 10.15480/882.9361

Eighth International Symposium on Marine Propulsors
smp'24, Berlin, Germany, March 2024

A Viscous Vorticity Model for Predicting Turbulent Flow over a Propeller

Rui You, Spyros A Kinnas

Ocean Engineering Group, Department of Civil, Architectural and Environmental Engineering The University of Texas at Austin, Austin, Texas 78712, USA

ABSTRACT

This paper extends the 3-D VIScous Vorticity Equation (VISVE) solver, originally designed for laminar flows, to address turbulence. By incorporating a $k-\omega$ SST turbulence model via the Finite Volume Method (FVM), the study aims to develop an efficient tool for analyzing propellers under realistic, turbulent conditions. The developed turbulent VISVE solver was applied to a 3-D NSRDC 4381 propeller with 5 blades. The VISVE method, with its spatially concentrated vorticity, allows for a highly efficient computational approach, significantly reducing computation time. The developed numerical model was validated with a Reynolds-Averaged Navier-Stokes (RANS) solver. Comparative analyses reveal substantial alterations in velocity and vorticity distributions between laminar and turbulent cases. Turbulence introduces complex flow patterns and thinner boundary layers, which the $k-\omega$ SST turbulence model captures. The extension of the VISVE method enhances predictions of propeller performance under real-world operating conditions. This study emphasizes the importance of considering turbulence in propeller analysis and design, providing a computational tool for this problem.

Keywords

Viscous Vorticity Equation, Turbulence Modeling, Propeller, 3-D, Turbulent flow

1 INTRODUCTION

Marine propellers operate in turbulent flows, presenting a significant challenge for numerical analysis and design. Conventional linear and potential flow theories have limitations in predicting turbulent flows. Viscous flow methods, though capable of handling turbulence by incorporating a turbulence model, are often computationally intensive.

The primary objective of this paper is to develop an efficient viscous numerical solver for simulating turbulent flows around propellers. The VIScous Vorticity Equation (VISVE) numerical solver was previously developed to handle laminar flow problems. This paper aims to extend this solver to allow for turbulence modeling. The focus is on implementing the $k-\omega$ SST turbulence model in the 3-D version of the VISVE solver. The turbulence model is discretized using the Finite Volume Method (FVM), and a hybrid OpenMP/MPI parallelization strategy is adopted to fully leverage High-Performance Computing (HPC) resources.

Tian (2014), Tian and Kinnas (2015) solved the VIScous Vorticity Equation (VISVE) for laminar flows by using a finite volume method. Tian (2014) developed the VISVE solver for laminar flows. Laminar VISVE has been applied on 2-D and 3-D hydrofoils, circular cylinders, and propeller blades (see Tian and Kinnas (2015), Wu and Kinnas (2019), Wu and Kinnas (2021) and Wu et al (2021)). Kinnas (2023) derived the vorticity equation for turbulent compressible flows with variable viscosity. However, to capture the realistic flow behavior around propellers, it is essential to extend the analysis to turbulent regimes. This paper presents an extension of the VISVE method, originally applied to laminar flows, to incorporate turbulent flow conditions. A $k-\omega$ SST (Shear Stress Transport) turbulence model is implemented into the solver to accurately capture the turbulent characteristics of the flow. Yao and Kinnas (2019) coupled VISVE with a turbulence model in OpenFOAM, to solve the turbulent flow around a 2-D hydrofoil and cylinder. However, this coupling method did not solve for the turbulence in VISVE, and needed to read the turbulent viscosity from OpenFOAM at every time step, which meant that the VISVE solver could not solve the turbulent flow independently. This gap is filled by You and Kinnas (2022). The turbulent $k-\omega$ SST model is discretized and solved within the VISVE code, thus solving for turbulent flows independently. You and Kinnas (2022a, 2022b) applied the 2-D turbulent VISVE solver to hydrofoils cases and cylinder cases. You and Kinnas (2022c, 2023, 2024) then extended the 2-D turbulent VISVE solving scheme to 3-D for hydrofoil applications.

The VISVE method was applied to a 3-D Naval Ship Research and Development Center (NSRDC) 4381 propeller with 5 blades. The developed numerical solver is utilized to simulate the flow around a propeller under both laminar and turbulent conditions. The resulting velocity and vorticity fields are analyzed and compared to evaluate the impact of the inclusion of the turbulence model.

The spatial concentration of vorticity allows for a localized solver with a considerably smaller computational domain and fewer cells, resulting in significantly reduced computation time. The effect of other blades is considered in an

iterative manner, which is similar to the method used in PROPCAV and MPUF-3A. Only the flow on the key blade is needed to be modeled, resulting in easily built grids. For axisymmetric case: duplicate the variables of the key blade. For non-axisymmetric case: use the variables of the key blade at different blade angles.

The findings from this study highlight the importance of considering turbulent flow conditions in propeller analysis and design. The extension of the VISVE method to include a $k-\omega$ SST turbulence model allows for more accurate predictions of propeller performance under realistic operating conditions. The comparative analysis between laminar and turbulent cases provides insights into the flow characteristics and their impact on propeller performance.

2 NUMERICAL MODELS

2.1 Vorticity Equation for 3-D Turbulent Flow

The 3-D VISVE Equation for variable density and viscosity is derived by Kinnas (2023):

$$\begin{aligned}&\frac{\partial\vec{\omega}}{\partial t}+\vec{\nabla}\times(\vec{\omega}\times\vec{q})\\&=\vec{\nabla}\times\left[-\vec{\nabla}\times(\nu\vec{\omega})+\vec{\nabla}\nu\times\vec{\omega}-\nabla^2\nu\vec{q}+\vec{\nabla}\times(\vec{q}\times\vec{\nabla}\nu)\right]\end{aligned}\tag{1}$$

For hydrofoil cases, $\frac{\partial\phi}{\partial x}<<\frac{\partial\phi}{\partial z}$, where ϕ can represent any variable, Equation (1) can be simplified as:

$$\frac{\partial\vec{\omega}}{\partial t}+\vec{\nabla}\times(\vec{\omega}\times\vec{q})=\vec{\nabla}\times\left[-\vec{\nabla}\times(\nu\vec{\omega})\right]\tag{2}$$

In comparison to the vorticity equation for laminar flow (Equation (3)), a notable distinction in the vorticity equation lies in the inclusion of the kinematic viscosity term (ν) inside the curl operator. This significant difference can lead to substantial variations in the obtained results.

$$\frac{\partial\vec{\omega}}{\partial t}+\vec{\nabla}\times(\vec{\omega}\times\vec{q})=\nu\vec{\nabla}\times\left[-\vec{\nabla}\times(\vec{\omega})\right]\tag{3}$$

2.2 Poisson Equation for Velocity Solver

Since the stream function in 2-D transforms into a vector in 3-D, presenting challenges in its treatment, which poses challenges in its handling, an alternative approach becomes necessary.

When solving the Navier-Stokes equations numerically, a common approach is to split them into pressure Poisson equation and velocity equations. The pressure equation is often obtained by taking the divergence of the momentum equation and imposing the incompressibility condition $\nabla\cdot q=0$. While the Poisson equation itself does not explicitly ensure a divergence-free velocity field, the pressure field helps correct the velocity field to maintain its divergence-free nature throughout the simulation.

Borrowing this idea, the same principle can potentially be applied to the Viscous Vorticity (VISVE) method to maintain divergence-free conditions.

Consider an arbitrary velocity field q, where its vorticity distribution is known as $\nabla\times q=\omega$. Now, imagine the existence of another vector field w, where its vorticity field also satisfies $\nabla\times w=\omega$, thus preserving the same vorticity distribution. Then the disparity between q and w can be interpreted in terms of a potential field:

$$\mathbf{q}=\mathbf{w}+\nabla\varphi\tag{4}$$

For potential flow, an irrotational velocity field v can be described by the gradient of the velocity potential $\nabla\varphi=v$. It means that the fluid particles are moving without any rotation or vorticity $\nabla\times\nabla\varphi=0$.

To prove that the difference between $\mathbf{q}$ and $\mathbf{w}$ is $\nabla\varphi$, we take the curl of both sides of the equation:

$$\nabla\times\mathbf{q}=\nabla\times(\mathbf{w}+\nabla\varphi)$$

Using the vector identity $\nabla\times\nabla\varphi=0$ (curl of a gradient is zero), we have:

$$\nabla\times\mathbf{q}=\nabla\times\mathbf{w}$$

The conclusion is that the potential term $\nabla\varphi$ does not alter the vorticity distribution.

To enforce continuity equation, which is $\nabla\cdot\mathbf{q}=0$, we take the divergence of Equation (4):

$$\nabla\cdot\mathbf{q}=\nabla\cdot\mathbf{w}+\nabla^2\varphi=0\tag{5}$$

Then, the Poisson's equation for φ is obtained:

$$\nabla^2\varphi=-\nabla\cdot\mathbf{w}\tag{6}$$

Equation (6) represents the Poisson equation we are addressing to solve for the velocity. The unknown in this equation is the velocity potential φ.

The following explains how the vorticity preserving field $\mathbf{w}^{n+1}$ is determined.

Consider the requirement of $\mathbf{w}^{n+1}$,

$$A\boldsymbol{\omega}^{n+1}\cdot\mathbf{n}=\sum_{\partial A}\mathbf{w}^{n+1}\cdot\Delta\mathbf{l}\tag{7}$$

For cell faces not adjacent to the wall, $\boldsymbol{\omega}^{n+1}=\boldsymbol{\omega}^{n+1*}$, since the vorticity creation only affects the first layer of cells. Recall

$$\begin{aligned}&A\boldsymbol{\omega}^{n+1}\cdot\mathbf{n}\\&=\Delta t\sum_{\partial A}\left[-\left(\boldsymbol{\omega}^{n+1*}\times\mathbf{q}^{n}\right)+\nabla\times\nu\boldsymbol{\omega}^{n+1*}\right]\cdot\Delta\mathbf{l}\\&+A\boldsymbol{\omega}^{n}\cdot\mathbf{n}\end{aligned}\tag{8}$$

and

$$A\boldsymbol{\omega}^{n}\cdot\mathbf{n}=\sum_{\partial A}\mathbf{q}^{n}\cdot\Delta\mathbf{l}\tag{9}$$

Comparing Equations (7), (8) and (9), we have

$$\mathbf{w}^{n+1}=\Delta t\left[-\left(\boldsymbol{\omega}^{n+1*}\times\mathbf{q}^{n}\right)+\nabla\times\nu\boldsymbol{\omega}^{n+1*}\right]+\mathbf{q}^{n}\tag{10}$$

For the cell face adjacent to the wall, the newly created vorticity has to be considered. It can be easily shown that

following construction for the edges on the wall recovers the ω^{n+1} in the first layer of cells:

$$\begin{aligned}\mathbf{w}^{n+1} =&\Delta t\left[-\left(\boldsymbol{\omega}^{n+1*}\times\mathbf{q}^{n}\right)+\nabla\times\nu\boldsymbol{\omega}^{n+1*}\right]\\&+\mathbf{q}^{n}+\mathbf{q}_{s}^{n+1*}+\nabla_{s}\phi^{n+1}\end{aligned}\tag{11}$$

Both (10) and (11) are explicit, because all the terms in the RHS are known once $\boldsymbol{\omega}^{n+1}$ is known.

where the normal gradient of φ can be evaluated as:

$$\begin{aligned}\left.\frac{\partial\varphi}{\partial n_{s1}}\right|_{i+1/2,j,k}&=\frac{\varphi_{i+1,j,k}-\varphi_{i,j,k}}{\Delta l_1|_{i+1/2,j,k}}+O\left(\Delta l^2\right)\\\left.\frac{\partial\varphi}{\partial n_{s1}}\right|_{i-1/2,j,k}&=\frac{\varphi_{i,j,k}-\varphi_{i-1,j,k}}{\Delta l_1|_{i-1/2,j,k}}+O\left(\Delta l^2\right)\\\left.\frac{\partial\varphi}{\partial n_{s2}}\right|_{i,j+1/2,k}&=\frac{\varphi_{i,j+1,k}-\varphi_{i,j,k}}{\Delta l_2|_{i,j+1/2,k}}+O\left(\Delta l^2\right)\\\left.\frac{\partial\varphi}{\partial n_{s2}}\right|_{i,j-1/2,k}&=\frac{\varphi_{i,j,k}-\varphi_{i,j-1,k}}{\Delta l_2|_{i,j-1/2,k}}+O\left(\Delta l^2\right)\\\left.\frac{\partial\varphi}{\partial n_{s3}}\right|_{i,j,k+1/2}&=\frac{\varphi_{i,j,k+1}-\varphi_{i,j,k}}{\Delta l_3|_{i,j,k+1/2}}+O\left(\Delta l^2\right)\\\left.\frac{\partial\varphi}{\partial n_{s3}}\right|_{i,j,k-1/2}&=\frac{\varphi_{i,j,k}-\varphi_{i,j,k-1}}{\Delta l_3|_{i,j,k-1/2}}+O\left(\Delta l^2\right)\end{aligned}\tag{12}$$

Equation (13) is the discretization of the Poisson equation for velocity applying the finite volume method.

$$\begin{aligned}&B_P\varphi_{i,j,k}+B_W\varphi_{i+1,j,k}+B_E\varphi_{i-1,j,k}+B_N\varphi_{i,j+1,k}\\&+B_S\varphi_{i,j-1,k}+B_T\varphi_{i,j,k+1}+B_B\varphi_{i,j,k+1}=-\dot{m}_{i,j,k}\end{aligned}\tag{13}$$

where,

$$\begin{aligned}B_W&=\left.\frac{A_s}{V\Delta l_1}\right|_{i+1/2,j,k},\quad B_E=\left.\frac{A_s}{V\Delta l_1}\right|_{i-1/2,j,k}\\B_N&=\left.\frac{A_s}{V\Delta l_2}\right|_{i,j+1/2,k},\quad B_S=\left.\frac{A_s}{V\Delta l_2}\right|_{i,j-1/2,k}\\B_T&=\left.\frac{A_s}{V\Delta l_3}\right|_{i,j,k+1/2},\quad B_B=\left.\frac{A_s}{V\Delta l_3}\right|_{i,j,k-1/2}\\B_P&=-\left(B_W+B_E+B_N+B_S+B_T+B_B\right)\end{aligned}\tag{14}$$

and

$$\begin{aligned}\dot{m}_{i,j,k}=&\left[\left(A_s\mathbf{w}\cdot\mathbf{n}_{s1}\right)_{i+1/2,j,k}-\left(A_s\mathbf{w}\cdot\mathbf{n}_{s1}\right)_{i-1/2,j,k}\right.\\&+\left(A_s\mathbf{w}\cdot\mathbf{n}_{s2}\right)_{i+1/2,j,k}-\left(A_s\mathbf{w}\cdot\mathbf{n}_{s2}\right)_{i-1/2,j,k}\\&\left.+\left(A_s\mathbf{w}\cdot\mathbf{n}_{s3}\right)_{i+1/2,j,k}-\left(A_s\mathbf{w}\cdot\mathbf{n}_{s3}\right)_{i-1/2,j,k}\right]/V\end{aligned}\tag{15}$$

2.3 Rotational Frame of Reference

When simulating propeller flow, it is advantageous to employ a rotational frame of reference. However, it's important to note that the uniform vorticity caused by the background rotation should be removed from the vorticity field when solving for VISVE.

In the case of a right-handed propeller functioning at a rotational speed of Ω, the rotational velocity vector can be represented as $(-\Omega,0,0)$. If we denote this rotational velocity as $\boldsymbol{\Omega}=(\Omega,0,0)$, then it can be expressed as follows:

$$\mathrm{q}_r=\mathrm{q}_a+\boldsymbol{\Omega}\times\mathbf{r}\tag{16}$$

where $\mathbf{q}_a$ is the velocity under the inertial frame of reference, and $\mathbf{q}_r$ is the velocity in the rotational frame of reference. $\mathbf{r}=(0,y,z)$ is the radial vector of a field point. The vorticity ω is defined under the inertial frame of reference:

$$\boldsymbol{\omega}=\nabla\times\mathbf{q}_a\tag{17}$$

The background rotation add a constant vorticity $2\boldsymbol{\Omega}$ into the relative velocity field $\mathbf{q}_r$:

$$\boldsymbol{\omega}+2\boldsymbol{\Omega}=\nabla\times\mathbf{q}_r\tag{18}$$

The momentum equation in the rotational frame of reference is written as:

$$\frac{\partial\mathbf{q}_r}{\partial t}+\mathbf{q}_r\cdot\nabla\mathbf{q}_r-2\boldsymbol{\Omega}\times\mathbf{q}_r-\Omega^2\mathbf{r}=-\nabla P+\nu\nabla^2\mathbf{q}_r\tag{19}$$

Substituting Equation (18) into Equation (19), with some manipulation, we have

$$\frac{\partial\mathbf{q}_r}{\partial t}+\nabla\left(\frac{q_r^2}{2}+P-\frac{\Omega^2r^2}{2}\right)=\mathbf{q}_r\times\boldsymbol{\omega}+\nu\nabla^2\mathbf{q}_r\tag{20}$$

Taking the curl of Equation (20) gives the VISVE in the rotational frame of reference:

$$\frac{\partial\boldsymbol{\omega}}{\partial t}+\nabla\times(\boldsymbol{\omega}\times\mathbf{q}_r)=-\nabla\times(\nabla\times\nu\boldsymbol{\omega})\tag{21}$$

Equation (21) reveals that, in the rotational frame of reference, the VISVE maintains its original form as observed in the inertial frame of reference. However, it is crucial to note that the velocity term within the VISVE should represent the relative velocity denoted as $\mathbf{q}_r$. It is worth highlighting that in the vorticity-velocity solver, the vector $\mathbf{w}$ does not incorporate the vorticity associated with the background rotation of $2\boldsymbol{\Omega}$. Consequently, when solving Poisson's equation for $\mathbf{q}_r$, it becomes necessary to incorporate the contribution of $2\boldsymbol{\Omega}$ into the vector $\mathbf{w}$.

Consider an edge with two nodes, where node one is represented as $\mathbf{x}_1=(x_1,y_1,z_1)$ and node two as $\mathbf{x}_2=(x_2,y_2,z_2)$. The contribution of the background rotation on this edge to the vorticity-preserving field, denoted as $\mathbf{w}$, can be described as follows:

$$\begin{aligned}\mathbf{w}_b\cdot\Delta\mathbf{l}&=\int_{\mathbf{x}_1}^{\mathbf{x}_2}\boldsymbol{\Omega}\times\mathbf{r}\cdot\mathrm{d}\mathbf{l}\\&=\boldsymbol{\Omega}\left(y_1z_2-z_1y_2\right)\end{aligned}\tag{22}$$

where, $\mathbf{w}_b$ represents an additional correction applied to $\mathbf{w}$ due to the background rotation. When utilizing the rotational frame of reference, it is necessary to include $\mathbf{w}_b$ into $\mathbf{w}$ calculated using the vorticity-velocity solver before invoking the Poisson solver for velocity.

As the Poisson solver is associated with $\mathbf{q}_r$, it is essential to account for the background rotation in the Neumann boundary condition as well. Therefore, ψ_b must be adjusted as follows:

$$\psi_b=\left(-\frac{1}{2}\Omega r^2,xU_{\infty,z}-zU_{\infty,x},0\right)\tag{23}$$

2.4 $k-\omega$ SST Turbulence Model

To incorporate the turbulence effects into the VISVE model, several crucial aspects need to be addressed. Apart from the modifications in the vorticity transport equation and the vorticity and velocity solver, one of the most critical considerations is determining the turbulent viscosity. By employing a suitable turbulence model, it becomes possible to account for the effects of turbulence and its impact on the flow variables.

In this context, ω' refers to the specific dissipation rate from the $k-\omega$ SST turbulence model, and should be distinguished from the vorticity ω in the previous VISVE model.

$k-\omega$ SST model proposed by Menter (1994) belongs to a two-equation eddy viscosity model. It is composed of two transport equations for turbulent kinetic energy k (Equation (24)) and specific dissipation rate ω' (Equation (25)).

$$\frac{\partial k}{\partial t}+U_j\frac{\partial k}{\partial x_j}=P-\beta^* k\omega'+\frac{\partial}{\partial x_j}\left[\left(\nu+\sigma_k\nu_T\right)\frac{\partial k}{\partial x_j}\right] \quad (24)$$

$$\frac{\partial \omega'}{\partial t}+U_j\frac{\partial \omega'}{\partial x_j}=\frac{\gamma}{\nu_T}P-\beta\omega'^2+\frac{\partial}{\partial x_j}\left[\left(\nu+\sigma_{\omega'}\nu_T\right)\frac{\partial \omega'}{\partial x_j}\right]+2\left(1-F_1\right)\sigma_{\omega'2}\frac{1}{\omega'}\frac{\partial k}{\partial x_i}\frac{\partial \omega'}{\partial x_i} \quad (25)$$

where k is the turbulent kinetic energy and ω' is the specific dissipation rate. P is the production for turbulent kinetic energy or dissipation rate:

$$P=\min\left(\frac{1}{\rho}\tau_{ij}\frac{\partial U_i}{\partial x_j},10\beta^* k\omega'\right) \quad (26)$$

where the Reynolds stress tensor $\tau_{ij}=2\mu_T S_{ij}-\frac{2}{3}\rho k\delta_{ij}$. For incompressible flow, P can be written as: $P=\frac{1}{\rho}\tau_{ij}\frac{\partial U_i}{\partial x_j}=\frac{1}{\rho}\tau_{ij}S_{ij}=2\nu_T S_{ij}S_{ij}$, where, mean rate of strain $S_{ij}=\frac{1}{2}\left(\frac{\partial U_i}{\partial x_j}+\frac{\partial U_j}{\partial x_i}\right)$.

The improved performance of the $k-\omega$ SST model is achieved through modifications in the eddy viscosity, primarily in the computation of the blending functions F_1 and F_2, as well as the inclusion of an additional cross-diffusion term. These blending functions can transform the standard $k-\omega$ model near the wall, to a high Reynolds number version of the $k-\epsilon$ model in the outer portion of the boundary layer.

$$F_1=\tanh\left\{\left\{\min\left[\max\left(\frac{\sqrt{k}}{\beta^*\omega' y},\frac{500\nu}{y^2\omega'}\right),\frac{4\sigma_{\omega'2}k}{CD_{k\omega'}y^2}\right]\right\}^4\right\} \quad (27)$$

$$F_2=\tanh\left[\left[\max\left(\frac{2\sqrt{k}}{\beta^*\omega' y},\frac{500\nu}{y^2\omega'}\right)\right]^2\right] \quad (28)$$

$$CD_{k\omega'}=\max\left(2\rho\sigma_{\omega'2}\frac{1}{\omega'}\frac{\partial k}{\partial x_i}\frac{\partial \omega'}{\partial x_i},10^{-10}\right) \quad (29)$$

where y is the distance from the wall. Let ϕ_1 be the constants in the $k-\omega$ model; ϕ_2 be the constants in the $k-\epsilon$ model, and ϕ is the corresponding constants of the $k-\omega$ SST model (ϕ can be γ, β, σ and α). The relation between them is:

$$\phi=\phi_1 F_1+\phi_2\left(1-F_1\right) \quad (30)$$

The coefficients prescribed for the $k-\omega$ SST model are used: $\kappa=0.41$, $\alpha_1=\frac{5}{9}$, $\alpha_2=0.44$, $\beta_1=\frac{3}{40}$, $\beta_2=0.0828$, $\beta^*=\frac{9}{100}$, $\sigma_{k1}=0.85$, $\sigma_{k2}=1$, $\sigma_{\omega'1}=0.5$, $\sigma_{\omega'2}=0.856$. $\gamma_1=\frac{\beta_1}{\beta^*}-\frac{\sigma_{\omega'1}\kappa^2}{\sqrt{\beta^*}}$, $\gamma_2=\frac{\beta_2}{\beta^*}-\frac{\sigma_{\omega'2}\kappa^2}{\sqrt{\beta^*}}$.

After solving Equation (24) and Equation (25), the kinematic turbulent viscosity can be obtained in the following way:

$$\nu_T=\frac{a_1 k}{\max\left(a_1\omega', SF_2\right)} \quad (31)$$

where $S=\sqrt{2S_{ij}S_{ij}}$.

2.5 Numerical Implementation for 3-D Turbulence Model

2.5.1 Discretization of $k-\omega$ sst model

Similar as to what have been done in 2-D, the 3-D $k-\omega$ SST model was discretized numerically based on the FVM method. A detailed derivation can be found in the appendix.

$$\left.\frac{\partial k}{\partial t}\right|_P\Omega=-\sum_f \overrightarrow{q_f}\cdot\overrightarrow{n_f}k_f s_f+\sum_f\left(\nu+\sigma_k\nu_T\right)_f\left.\frac{\partial k}{\partial n}\right|_f s_f+\bar{S}\big|_P\Omega \quad (32)$$

2.5.2 Green-Gauss cell-based gradient evaluation

When dealing with structured orthogonal grids, calculating the gradient of a scalar at a control volume centroid is straightforward using the definition of derivatives. However, for general unstructured grids, the process becomes more complex. In such cases, the Green-Gauss theorem is commonly used as a numerical method. This theorem relates the surface integral of a scalar function to the volume integral of the gradient of the scalar function.

To compute the average face value, which is necessary for accurate computation of the cell gradient, there are two main approaches: cell-based and node-based. In the cell-based approach, the face value is computed using the values at its surrounding cells. This method is particularly suitable for structured grids. On the other hand, the node-based approach computes the face value using the values at its surrounding nodes. This method is more suitable for unstructured grids.

It's worth mentioning that these methods are not specific to gradient computation and can be used whenever the face value is required in numerical calculations. They provide a way to approximate the average value at a face using the values of neighboring cells or nodes, depending on the approach chosen.

2.5.3 PARDISO matrix solver

PARDISO, developed by Intel Corporation, is a direct solver specifically designed for solving large sparse linear systems of equations. It is based on the multifrontal method, which is a direct method for solving large sparse linear systems. PARDISO takes advantage of modern computer architectures, such as multi-core processors and parallel computing, to efficiently solve large-scale linear systems. It is widely used in scientific and engineering applications and is known for its high performance and accuracy.

While PARDISO is a direct solver, it is also designed to efficiently handle large matrices by exploiting their sparsity structure. Large sparse matrices are common in many scientific and engineering applications, and direct solvers can be computationally expensive and memory-intensive to solve these problems directly. However, PARDISO overcomes these challenges by utilizing techniques such as parallel processing, memory management, and matrix reordering to reduce the computational and memory requirements of the direct solver algorithm.

2.5.4 MPI/OpenMP hybrid parallelization

In order to achieve optimal performance on multi-core and multi-processor systems, it is crucial to fully utilize the features of parallelism and efficiently manage the memory hierarchy.

MPI (Message Passing Interface) applications can facilitate scalability across multiple SMP (Symmetric Multiprocessing) nodes. OpenMP applications can improve the efficient utilization of shared memory on SMP nodes. By incorporating MPI and OpenMP during the coding process, efficiency, performance, and scaling can be maximized. Hybridization refers to a method of employing different parallelization models to leverage the advantages of each.

3 APPLICATION

3.1 Geometry of the NSRDC 4381 Propeller

As shown in Figure 1, the Naval Ship Research and Development Center (NSRDC) 4381 propeller (Boswell 1971) has been employed in this test. The geometry is specified with respect to a right-handed, blade fixed coordinate system, with the x-axis pointing downstream. The propeller was assumed to operate in an incompressible, steady flow regime, with inflow equal to 1 m/s.

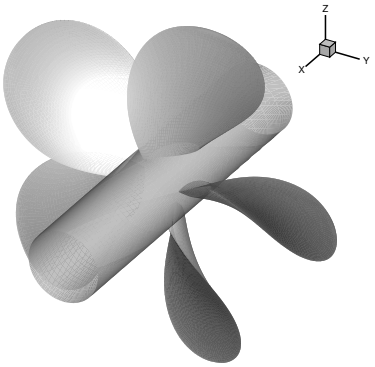

Figure 1. The NSRDC 4381 propeller with 5 blades.

Table 1 provides important design parameters for a propeller. It specifies that the propeller has 5 blades and an expanded area ratio of 0.725. The section meanline follows the NACA a=0.8 distribution, indicating the shape of the propeller sections. The section thickness distribution is NACA66 with NSRDC modified nose and tail, suggesting modifications made to the standard NACA66 thickness distribution. The design advance ratio $J = V/nD$ of this propeller is 0.889, where V is the ship speed, n is the rotational speed of the propeller in revolution per second, and D is the diameter of the propeller.

Table 1. Propeller design parameters.

Parameter	Value
Number of Blades	5
Expanded Area Ratio	0.725
Section Meanline	NACA a=0.8
Section Thickness Distribution	NACA66 with NSRDC modified nose and tail
Design J	0.889

Table 2 provides the values of various parameters of the 4381 propeller at a projected skew angle of $\theta_s = 0$ degrees. The table includes the hydrodynamic pitch angle β_i, section chord length c, propeller section pitch P/D, and section camber f/c.

Table 2. The geometry of NSRDC 4381 propeller with 0 degree skew angle.

r/R	$\tan\beta_i$	c/D	t/C	P/D	f/c
0.3	1.3094	0.229	0.1562	1.3448	0.0368
0.4	1.0075	0.275	0.1068	1.3580	0.0348
0.5	0.8034	0.312	0.0768	1.3361	0.0307
0.6	0.6483	0.337	0.0566	1.2797	0.0245
0.7	0.5300	0.347	0.0421	1.2099	0.0191
0.8	0.4390	0.334	0.0314	1.1366	0.0148
0.9	0.3681	0.280	0.0239	1.0660	0.0123

3.2 Computational Settings

3.2.1 Computational settings in VISVE

In VISVE, a structured, multi-block mesh with hexahedral elements was generated to accurately capture the complex geometry of the propeller and its surrounding fluid domain. The mesh refinement was performed near the blade surfaces and in regions of high flow gradients to ensure sufficient resolution.

For turbulence modeling, the SST $k-\omega$ turbulence model was employed, as it has demonstrated good performance for predicting the flow characteristics around marine propellers. The simulation was conducted using a time step size of 10^{-4} seconds.

The significance of the mesh generation procedure in the VISVE solver lies in its simplicity and user-friendliness. Unlike commercial mesh tools that can be complex and require detailed specifications, the VISVE solver offers an

easy-to-use approach for generating grids. By simply inputting the desired number of blocks, the grid can be quickly and efficiently generated, making the entire process much more accessible to researchers and engineers.

For a propeller or turbine, VISVE only models an individual blade without the necessity of modeling the space between blades. In contrast, velocity-based methods typically require a significant amount of user time to create a suitable grid with a smooth transition from the grids around one blade to those around the adjacent blade.

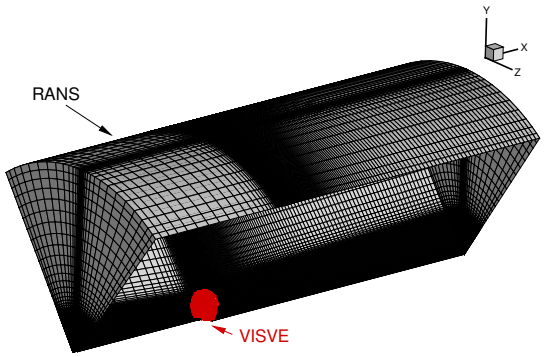

Figure 2. Comparison of the computational domain between VISVE and RANS for the NSRCD 4381 propeller.

Table 3 illustrates a comparison on the number of grids and the computational time required per iteration between the VISVE and RANS models for the propeller case. With 40 CPUs allocated to both cases, the VISVE method exhibits four times the speed of the RANS method.

Table 3. Comparison of the mesh and the computational time between VISVE and RANS for the propeller.

	VISVE	RANS
Mesh	243,000	3,364,522
Computational time/iter	10.5 s	37 s
No. of CPUs	40	40

Figure 3 shows the mesh configuration on the key blade of the propeller from different views. The top view displays the mesh arrangement on the upper surface of the propeller blade. The bottom view shows the mesh layout on the lower surface of the propeller blade. The side view provide the distribution of mesh elements along the span of the blade, providing insights into the discretization of the computational domain in the vertical direction. A well-structured and refined mesh is essential for accurately capturing the flow behavior around the propeller blade, including the boundary layer. The spatial concentration of vorticity allows for a localized solver with a considerably smaller computational domain and fewer cells, resulting in significantly reduced computation time.

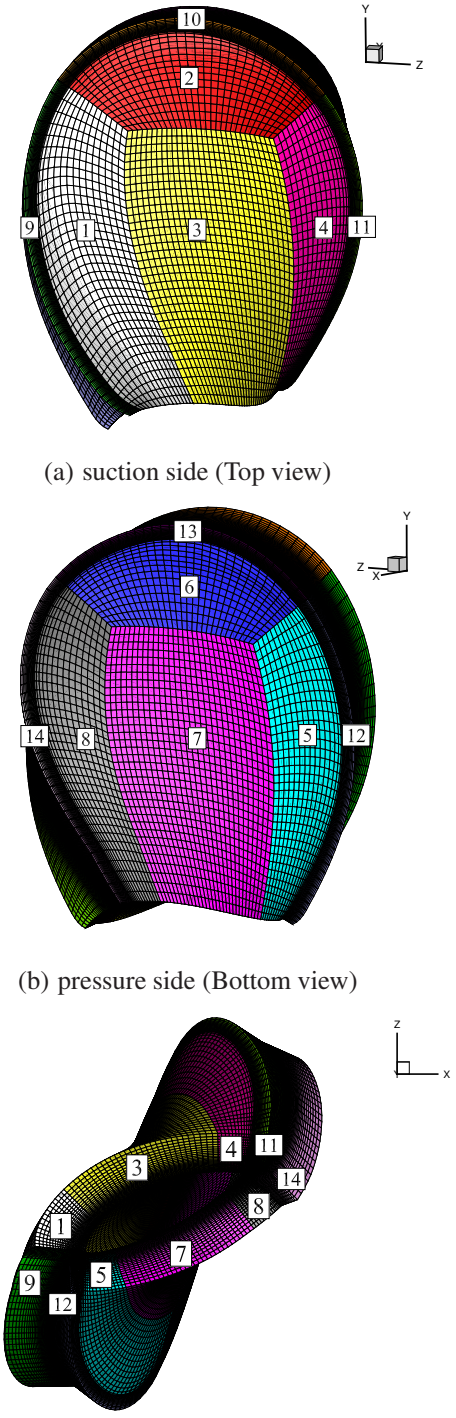

(a) suction side (Top view)

(b) pressure side (Bottom view)

(c) Side view

Figure 3. Mesh on the key blade of the propeller.

3.3 Validation with a RANS solver

The comparison between VISVE and RANS results, regarding the velocity profiles are conducted in this section. Figures 4 - 7 show the comparison of velocity profiles between VISVE and RANS at different locations. V1, V2, and V3 denote the velocity components in the chordwise, radial, and spanwise directions, respectively. y/c represents the spanwise location, and x/c represents the chordwise location. The figures illustrate the boundary layer profiles normal to each of these locations.

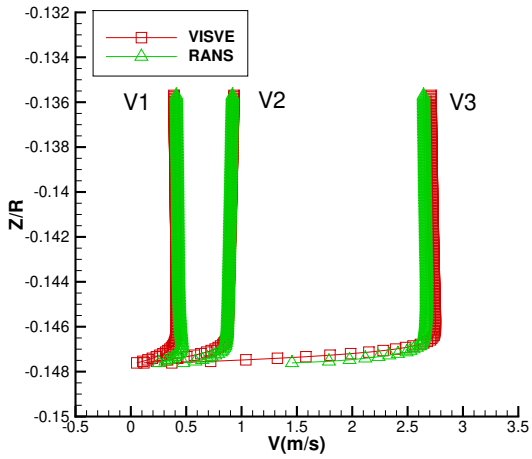

Figure 4. Comparison of velocity profiles between VISVE and unsteady RANS, y/c=0.9, x/c=0.2, Re=1 × 10^6, J=1.1.

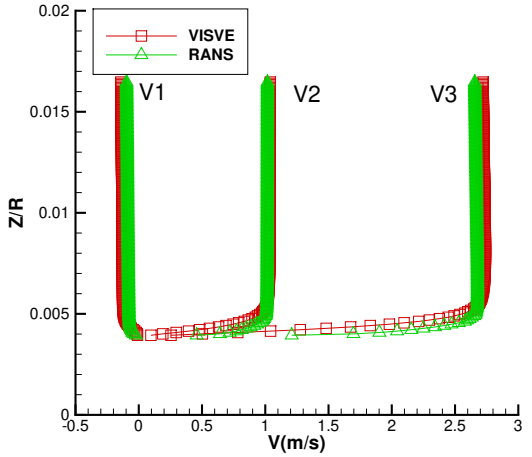

Figure 5. Comparison of velocity profiles between VISVE and unsteady RANS, y/c=0.9, x/c=0.5, Re=1 × 10^6, J=1.1.

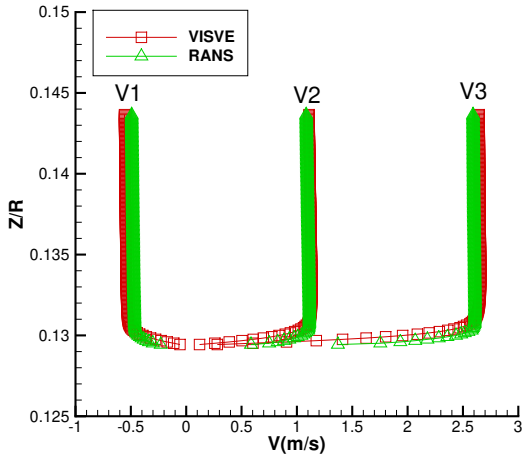

Figure 6. Comparison of velocity profiles between VISVE and unsteady RANS, y/c=0.9, x/c=0.8, Re=1 × 10^6, J=1.1.

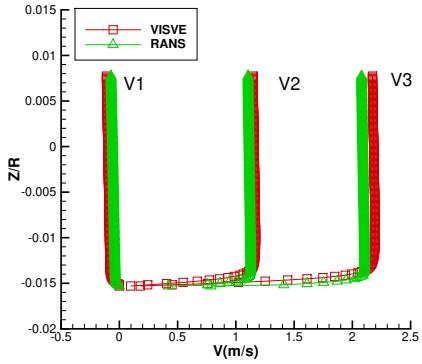

Figure 7. Comparison of velocity profiles between VISVE and unsteady RANS, y/c=0.7, x/c=0.5, Re=1 × 10^6, J=1.1.

3.4 Comparison between laminar and turbulent VISVE solver

Figure 8 shows the comparison of vorticity profile between laminar and turbulent VISVE solver at x/R=0.5, y/R=0.5. Comparative analyses are performed to assess the differences in velocity distributions between the laminar and turbulent cases in Figure 9 - Figure 11. Laminar VISVE indicates that the simulation is conducted without a turbulence model, but with a Reynolds number of 10^6; hence, the flow is not in a laminar regime. The aim of this figure is to demonstrate the significance of including a turbulence model. Please note that Please note that this is not a figure comparing the laminar and turbulent boundary layer, as in that case, the turbulent boundary layer is much thicker than laminar boundary layer. The results demonstrate that the turbulent flow regime significantly alters the flow field near the propeller, potentially leading to changes in performance and overall propeller behavior. For the results predicted by the laminar solver, the flow remains smooth and orderly, with gradual changes in velocity and vorticity. However, for the results predicted by the turbulent VISVE solver, the flow exhibits complex flow patterns and thinner boundary layers. The addition of the $k-\omega$ SST turbulence model enables the accurate prediction of these turbulent effects.

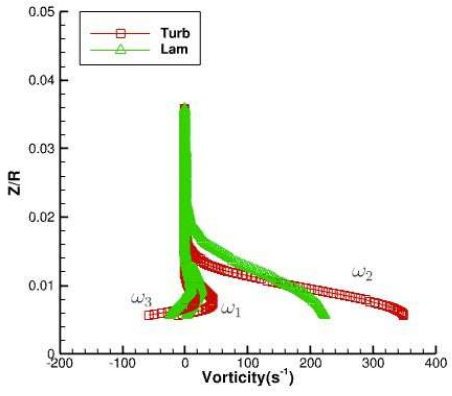

Figure 8. Comparison of vorticity profile between laminar and turbulent VISVE solver, x/R=0.5, y/R=0.5, Re=1 × 10^6.

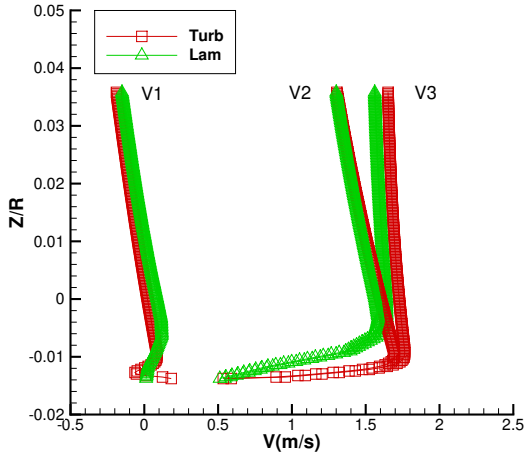

(a) x/R=0.2

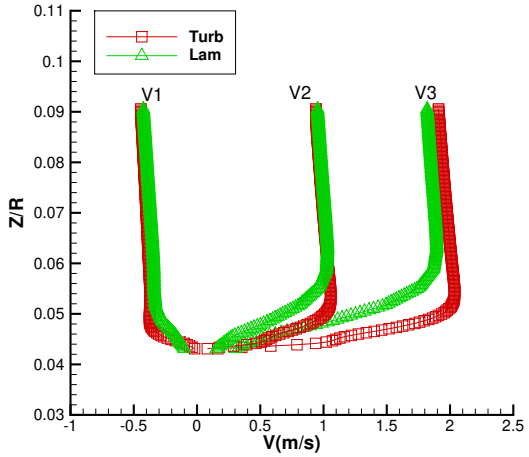

(b) x/R=0.5

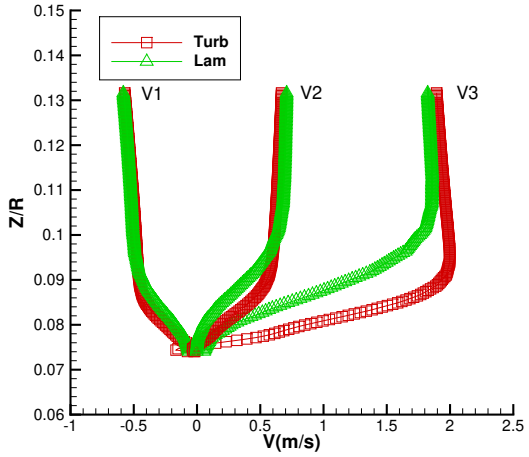

(c) x/R=0.8

Figure 9. Comparison of velocity profile between laminar and turbulent VISVE solver, y/R=0.2, Re=1 × 10^6.

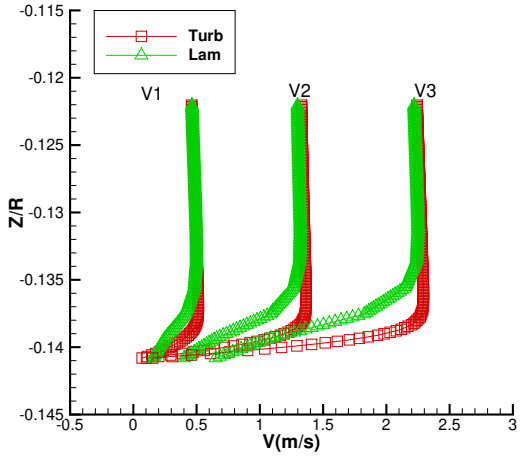

(a) x/R=0.2

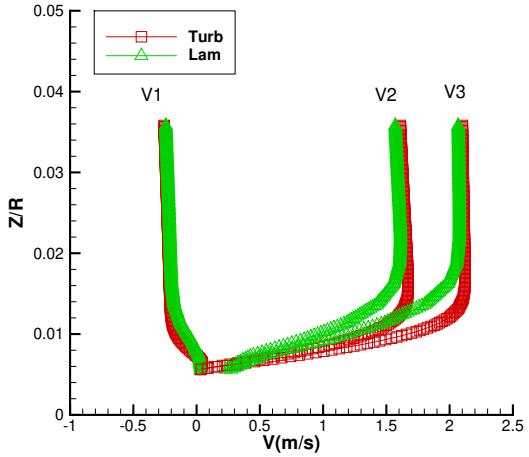

(b) x/R=0.5

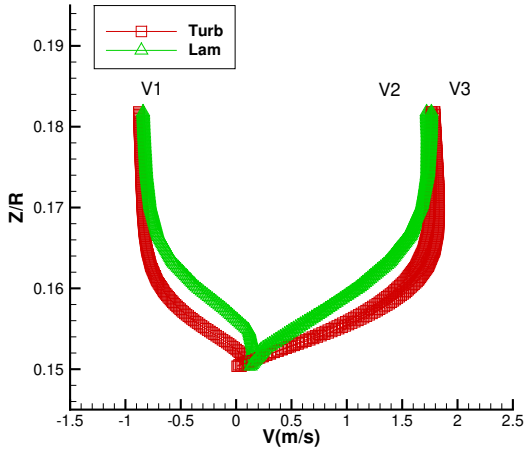

(c) x/R=0.8

Figure 10. Comparison of velocity profile between laminar and turbulent VISVE solver, y/R=0.5, Re=1 × 10^6.

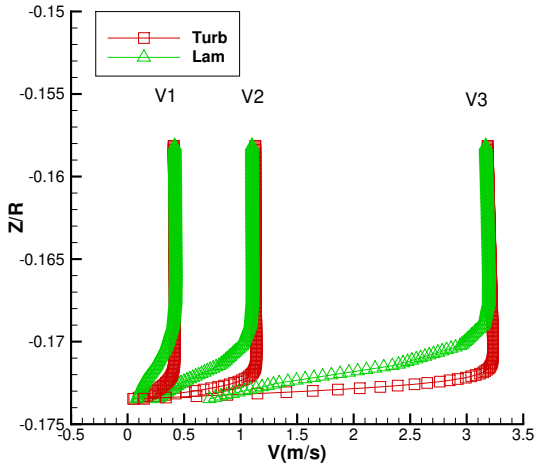

(a) x/R=0.2

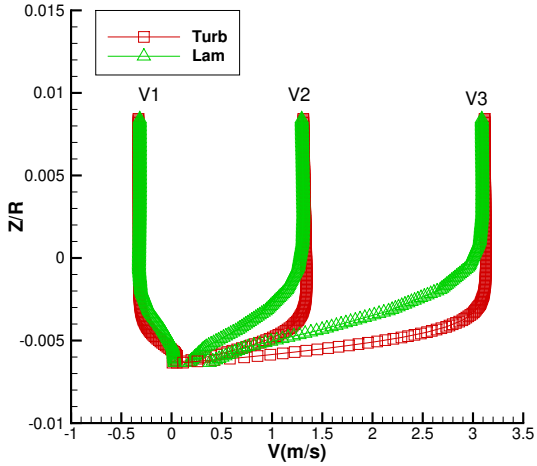

(b) x/R=0.5

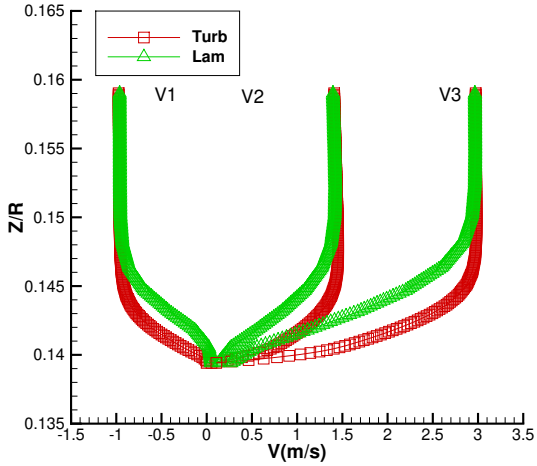

(c) x/R=0.8

Figure 11. Comparison of velocity profile between laminar and turbulent VISVE solver, y/R=0.8, Re=1 × 10^6.

4 CONCLUSIONS

In conclusion, this study has extended the 3-D VIScous Vorticity Equation (VISVE) method to address turbulent flow scenarios. By incorporating the $k-\omega$ SST turbulence model into the solver, we have developed a computational tool for simulating propeller behavior in turbulent flow conditions. The developed numerical model was validated with a Reynolds-Averaged Navier-Stokes (RANS) solver. The results highlight the disparities between laminar and turbulent flow cases, emphasizing the critical importance of considering turbulence in propeller analysis. The findings underscore the substantial impact of turbulence on flow behavior, with complex patterns and thinner boundary layers identified. The inclusion of the turbulence model ensures the prediction of these effects.

The authors plan to evaluate the pressures over the blades, and eventually predict the propeller performance (thrust, torque, and efficiency) at various advance coefficients. In addition, they plan on improving the computational efficiency of their method further.

ACKNOWLEDGMENTS

Support for this research was provided by the U.S. Office of Naval Research (Grant Numbers N00014-18-1-2276 and N00014-21-1-2488; Dr. Yin Lu Young) and by Phases VIII, and IX of the "Consortium on Cavitation Performance of High Speed Propulsors".

REFERENCES

Boswell, R. J. (1971). Design, cavitation performance, and open-water performance of a series of research skewed propellers. David W Taylor Naval Ship Research and Development Center Bethesda MD.

Kinnas, S. A. (2020). 'VIScous Vorticity Equation (VISVE) for Turbulent 2-D Flows with Variable Density and Viscosity'. Journal of Marine Science and Engineering **8**(3), pp.191.

Kinnas, S. A. (2023). 'VIScous Vorticity Equation (VISVE) for Turbulent 3-D Flows with Variable Density and Viscosity'. Under preparation.

Menter, F. R. (1994). 'Two-equation eddy-viscosity turbulence models for engineering applications'. AIAA journal **32**(8), pp.1598–1605.

Schenk, O. & Gärtner, K. (2004). 'Solving unsymmetric sparse systems of linear equations with PARDISO'. Physics of Fluids **20**(3), pp.475–487.

Tian, Y. & Kinnas, S. A. (2015). 'A viscous vorticity method for propeller tip flows and leading edge vortex'. Fourth international symposium on marine propulsors (smp15), Austin, Texas, USA.

Tian Y. (2014). Leading edge vortex modeling and its effect on propulsor performance. Dept. of Civil, Architectural and Environmental Engineering, The University of Texas at Austin, USA.

Wu, C. & Kinnas, S. A. (2019). 'A conservative viscous vorticity method for unsteady unidirectional and oscil-

latory flow past a circular cylinder'. Ocean Engineering **191**, pp.106504.

Wu, C., Kinnas, S. A., Li, Z. & Wu, Y. (2021). 'Parallel implementation of a VIScous Vorticity Equation (VISVE) method in 3-D laminar flow'. Journal of Computational Physics **426**, pp.109912.

Wu, C. & Kinnas, S. A. (2021). 'Flow past a rotating cylinder predicted by a compact Eulerian viscous vorticity method under non-inertial rotating frame'. Ocean Engineering **230**, pp.108882.

Yao, H. & Kinnas, S. A. (2019). 'Coupling Viscous Vorticity Equation (VISVE) Method with OpenFOAM to Predict Turbulent Flow around 2-D Hydrofoils and Cylinders'. Proceedings of the 29th International Ocean and Polar Engineering Conference, Hawaii, USA.

You, R. & Kinnas, S. A. (2022a). 'VIScous Vorticity Equation (VISVE) model applied to 2-D turbulent flow over hydrofoils'. Ocean Engineering **256**, pp.111416.

You, R. & Kinnas, S. A. (2022b). 'VIScous Vorticity Equation (VISVE) Model Applied to Oscillatory Turbulent Flow around a Cylinder'. SNAME 27th Offshore Symposium, Houston, USA.

You, R. & Kinnas, S. A. (2022c). 'A Viscous Vorticity Method for Predicting Lifting Surface Performance in Turbulent Flow Using a Two-Equation Turbulence Model'. Proceedings of 34th Symposium on Naval Hydrodynamics, Washington, D.C., USA.

You R. (2023). A Viscous Vorticity Method for the Prediction of Turbulent Flows around Hydrofoils and Propellers Dept. of Civil, Architectural and Environmental Engineering, The University of Texas at Austin, USA.

You, R. & Kinnas, S. A. (2024). 'A 3-D Viscous Vorticity Model for Predicting Turbulent Flows over Hydrofoils.' J. Mar. Sci. Eng. **12**, pp.45.